Taylor & Francis
Taylor & Francis Group

INVITED ARTICLE

Absorption spectra and aqueous photochemistry of β-hydroxyalkyl nitrates of atmospheric interest

Dian E. Romonosky[a], Lucas Q. Nguyen[a], Dorit Shemesh[b], Tran B. Nguyen[a], Scott A. Epstein[a], David B.C. Martin[a], Christopher D. Vanderwal[a], R. Benny Gerber[a,b] and Sergey A. Nizkorodov [a,*]

[a]Department of Chemistry, University of California, Irvine, CA, USA; [b]Fritz Haber Center for Molecular Dynamics, The Hebrew University, Jerusalem, Israel
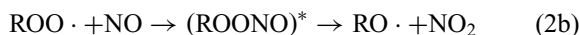
Molar absorption coefficients were measured for select alkyl nitrates and β-hydroxyalkyl nitrates in methanol. The presence of the β-hydroxyl group has a relatively minor effect on the absorption spectrum in the vicinity of the weak $n \rightarrow \pi^*$ transition, which is responsible for photolysis of organic nitrates in the atmosphere. For both alkyl nitrates and β-hydroxyalkyl nitrates, there is an enhancement in the absorption coefficients in solution compared to the gas-phase values. The effect of the β-hydroxyl group on the spectra was modelled with molecular dynamics simulations using an OM2/GUGA-CI Hamiltonian for ethyl nitrate and β-hydroxyethyl nitrate. The simulation provided a qualitatively correct shape of the low energy tail of the absorption spectrum, which is important for atmospheric photochemistry. The role of direct aqueous photolysis in removal of β-hydroxyalkyl nitrates in cloud and fog water was modelled using a relative rate approach, and shown to be insignificant relative to gas-phase photochemical processes and aqueous OH oxidation under typical atmospheric conditions.
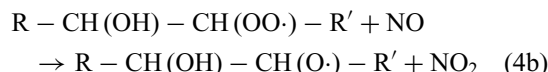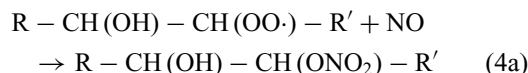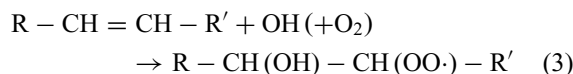
Keywords: molar absorption coefficients; molecular dynamics; aqueous photolysis; cloud processing of aerosols; organonitrates
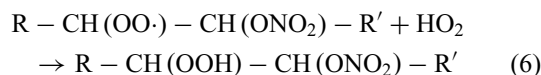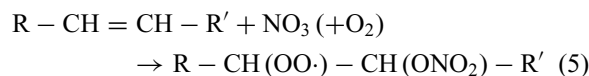
1. Introduction

Esters of nitric acid, better known as organic nitrates to atmospheric chemists, represent an important group of atmospheric organic compounds [1]. Oxidation of saturated hydrocarbons in air by OH in the presence of NO_x (NO + NO_2) is a common pathway to unsubstituted alkyl nitrates:

$$RH + OH\,(+O_2) \rightarrow ROO \cdot + H_2O \quad (1)$$

$$ROO \cdot + NO \rightarrow (ROONO)^* \rightarrow RONO_2 \quad (2a)$$

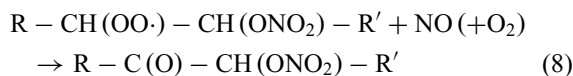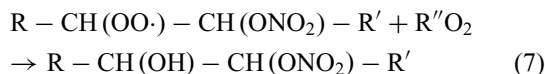$$ROO \cdot + NO \rightarrow (ROONO)^* \rightarrow RO \cdot + NO_2 \quad (2b)$$

The yield of reaction (2a) relative to that of reactions (2a + 2b) increases with the size of the alkyl group, R, and approaches ∼30% for larger peroxy radicals, ROO• [1]. Under the same conditions, the oxidation of unsaturated hydrocarbons commonly produces nitrates with a hydroxyl (–OH) group in the β position relative to the nitroxy (–ONO_2) group [2–5]:

$$R - CH = CH - R' + OH\,(+O_2)$$
$$\rightarrow R - CH(OH) - CH(OO\cdot) - R' \quad (3)$$

$$R - CH(OH) - CH(OO\cdot) - R' + NO$$
$$\rightarrow R - CH(OH) - CH(ONO_2) - R' \quad (4a)$$

$$R - CH(OH) - CH(OO\cdot) - R' + NO$$
$$\rightarrow R - CH(OH) - CH(O\cdot) - R' + NO_2 \quad (4b)$$

Reactions (3) and (4) are especially important in the oxidation of biogenically emitted isoprene, monoterpenes, and other unsaturated volatile organic compounds in air masses affected by urban emissions. The resulting β-hydroxyalkyl nitrates have been observed in significant concentrations in both urban and remote environments in a number of field studies [6–9]. Reactions of nitrate radicals with alkenes also serve as an important source of nitrates [10–16] substituted by a hydroxyl, hydroperoxyl (–OOH), or carbonyl group (= O) in the β-position, for example, through the following sequence of reactions:

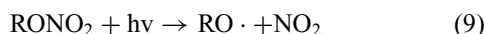$$R - CH = CH - R' + NO_3\,(+O_2)$$
$$\rightarrow R - CH(OO\cdot) - CH(ONO_2) - R' \quad (5)$$

$$R - CH(OO\cdot) - CH(ONO_2) - R' + HO_2$$
$$\rightarrow R - CH(OOH) - CH(ONO_2) - R' \quad (6)$$

---

*Corresponding author. Email: nizkorod@uci.edu

$$R - CH(OO\cdot) - CH(ONO_2) - R' + R''O_2$$
$$\rightarrow R - CH(OH) - CH(ONO_2) - R' \qquad (7)$$

$$R - CH(OO\cdot) - CH(ONO_2) - R' + NO(+O_2)$$
$$\rightarrow R - C(O) - CH(ONO_2) - R' \qquad (8)$$

Other pathways to β-substituted alkyl nitrates also exist. A comprehensive review of these mechanisms is beyond the scope of this paper.

For unsaturated nitrates, such as the ones derived from isoprene, reaction with OH serves as the most important daytime sink, while reaction with NO_3 dominates at night [17]. For saturated nitrates, other sink mechanisms may become competitive. One of the known degradation pathways for alkyl nitrates is gas-phase photolysis by means of the weak $n \rightarrow \pi^*$ transition [18,19]:

$$RONO_2 + h\nu \rightarrow RO\cdot + NO_2 \qquad (9)$$

The absorption cross sections [18–23] and photolysis quantum yields [24,25] of gas-phase alkyl nitrates have been studied extensively, making it possible to reliably predict the rate of reaction (9) under all relevant atmospheric conditions. The electronic states [26–30] and photodissociation dynamics [30–32] of simple alkyl nitrates have also been investigated. Because of the low oscillator strength of the $n \rightarrow \pi^*$ transition, the photolysis is relatively slow with typical lifetimes of days. In contrast to the simple alkyl nitrates, photochemistry of β-substituted nitrates is less well understood. Investigation of the neighbouring group effects on photochemistry of atmospheric organic compounds is important; for example, the synergetic interaction between the carbonyl and nitroxy groups on the neighbouring carbon atoms has been shown to lead to an efficient photolysis of β-carbonyl nitrates that occurs at faster rates than reaction with OH [33]. In the case of β-hydroxyalkyl nitrates, absorption cross sections have been measured only for a few compounds, such as β-hydroxyethyl nitrate [20] and trans-2-hydroxycyclopentyl-1-nitrate [34], and no photolysis studies have been done.

Depending on their solubility and volatility, organic nitrates can remain in the gas-phase, partition into cloud and fog droplets, or partition into aerosol particles. The presence of a hydroxyl group decreases the vapour pressure and increases the solubility of small β-hydroxyalkyl nitrates enough to make their wet and dry deposition a significant sink. The magnitudes of the measured Henry's solubility constants suggest that β-hydroxyalkyl nitrates partition into the aqueous phase to a significant extent whenever cloud and fog droplets are present [35,36]. Larger β-hydroxyalkyl nitrates, such as ones derived from the oxidation of monoterpenes, may have sufficiently low vapour pressures to efficiently partition into aerosols and onto environmental surfaces, especially if they are decorated

with additional functional groups. Indeed, there have been a number of observations of β-hydroxyalkyl nitrates in particle-phase products of oxidation of isoprene [37,38], alpha-pinene [3,14,39], and other terpenes.

Despite the fact that electronic excitations play a major role in the initiation of atmospheric reactions [1], theoretical predictions of the accurate shapes of the absorption spectra of atmospheric compounds remain a major challenge. Significant radiation is available in the lower atmosphere only for wavelengths longer than 290 nm (photon energies below 4.3 eV) because higher energy photons are efficiently screened by stratospheric ozone. For many atmospheric molecules, the lowest electronic transition is centred deeper in the ultraviolet (UV) region, and the absorption takes place in the red tail of the spectrum, far removed from the absorption centre. Even though the absorption coefficient in the red tail of the spectrum is small, it may dominate the atmospheric photochemistry because only the near-UV photons can make it through the ozone shield. The importance of weak red tails in absorption spectra of atmospheric molecules was stressed in a study of photochemistry of methyl hydroperoxide [40]. This situation applies to alkyl nitrates because their $n \rightarrow \pi^*$ transition is centred at $\sim$260 nm and only the tail of this transition overlaps with the tropospheric actinic wavelength region [21,26]. The calculation of the shape of the red tail of the spectrum requires considerable computational effort. The Franck–Condon region is greatly extended at ambient temperatures by the internal motion of the molecule making it necessary to calculate vertical electronic transition energies and oscillator strengths at various molecular geometries. In condensed phases, the tail absorption may be affected by the shift of the electronic states due to the presence of solvent molecules. References [41–43] provide illustrative examples of accounting for these effects in predictions of absorption spectra of atmospheric compounds. For a recent review on the applications of molecular dynamics (MD) methods to photochemical problems, the reader is referred to Ref. [44].

The main question addressed in this paper is whether direct photolysis of β-hydroxyalkyl nitrates in the aqueous phase or in the organic particle phase is atmospherically relevant. With several notable exceptions, such as measurements of molar absorption coefficients of simple alkyl nitrates in hexane [45] and photolysis of alkyl nitrates on ice surfaces [46], condensed-phase photochemistry of alkyl nitrates has not been studied enough to predict whether it can compete with gas-phase photochemistry or heterogeneous oxidation. In this study, we begin to address the following important questions by examining the molar absorption coefficients of atmospherically relevant β-hydroxyalkyl nitrates dissolved in methanol. Are solvatochromic effects significant for these types of molecules? Does the presence of the solvent affect the photolysis quantum yields? Do additional photolysis channels open up in the condensed

phase? Does the β-hydroxyl group play a special role in the photochemistry, e.g., by hydrogen bonding to the nitroxy group? In addition to the experimental measurements, we explore the effect of the β-hydroxyl group on the shape of the $n \rightarrow \pi^*$ band in ethyl nitrate and β-hydroxyethyl nitrate using on-the-fly molecular dynamics.

2. Methods

2.1. Experimental methods

The β-hydroxyalkyl nitrates labelled A-I in Table 1 were synthesised by nucleophilic epoxide ring opening with bismuth (III) nitrate [47].

The procedures included addition of the nucleophile at room temperature under inert atmosphere to a solution of the selected, reagent-grade epoxide and acetonitrile. The reaction was quenched with deionised water and the resulting β-hydroxyalkyl nitrates were collected by extraction with ethyl acetate. All nitrates were purified using liquid chromatography with a solvent system comprised of ethyl acetate and hexanes. Solvents were removed using a rotary evaporator. Proton nuclear magnetic resonance (NMR) was employed to verify the structure and purity of the resulting product. The compound obtained in the highest yield and purity was 2-hydroxycyclohexyl nitrate (A), which was in crystalline form. The rest of the compounds were obtained as viscous liquids, and judging by their yellowish colour, may have contained impurities (estimated to be under 5% based on NMR spectra) from the synthesis. Because of the possible presence of impurities we elected not to report molar absorption coefficients above 330 nm in this paper. Each sample was tested for the presence of nitrate and other functional groups using a Mattson GL-5030 Fourier-transform infrared spectroscopy (FTIR) spectrometer. A sample FTIR spectrum of 4-hydroxytetrahydrofuran-3-yl nitrate (F) is shown in Figure S1. The spectra were consistent with spectra of alkyl nitrates reported by Bruns *et al*. [48]; specifically the bands attributable to nitrates were observed at 1630, 1280, and 860 cm^{-1} for all compounds. For compound F, the OH stretching band associated with the hydroxyl group was also present (Figure S1). Nitrates were stored in a refrigerator at 5 °C. However, some of the compounds, e.g., 3-hydroxy-3-methylbutan-2-yl nitrate (B), were unstable under standard storage conditions. Therefore, we performed all the measurements shortly after the preparation. Nitrates labelled J, K, and L in Table 1 were purchased and used without further purification.

The ultraviolet-visible (UV-vis) absorption spectra were taken by a Shimazdu UV-2450 spectrometer with an accuracy of ± 0.003 absorbance units in the base-10 absorbance range of 0–1. Each sample was scanned in the 200–700 nm wavelength range with a rate of 210 nm/min. Each experimental run involved taking spectra for several volume dilutions of the nitrate in methanol (the only exception to

that was compound L that was studied in multiple solvents). To improve baseline stability, the spectra were baseline-corrected by setting the average measured absorbance in the 500–700 nm range to zero. We acknowledge that it would be preferable to investigate the absorption spectra in water. However, we elected to use methanol as the solvent because of the limited water solubility of the nitrates examined in this work. Methanol is a reasonably polar solvent, and we expect that its effects on the absorption spectra should be comparable to that of water.

2.2. Theoretical methods

The structures were built in Avogadro [49,50], a program that includes a minimisation procedure with MMFF94 force field and a conformer search option. The identified conformers were further optimised at Møller-Plesset second order perturbation (MP2) theory level using the resolution of identity approximation [51]. The correlation-consistent polarized valence double-zeta (cc-pVDZ) basis set was employed [52]. Vertical excitation energies were computed with the with second-order approximate coupled-cluster (CC2) method [53,54] at the MP2 optimised structures. For some conformers, the vertical excitation energies were also computed with the orthogonalisation-corrected orthogonalization method 2 (OM2) Hamiltonian [55] and the multireference configuration interaction procedure using the graphical unitary group approach (GUGA-CI) [56] using the modified neglect of diatomic overlap (MNDO) program [57]. In GUGA-CI calculations, three reference configurations were used (closed shell, single, and double highest occupied molecular orbital (HOMO) to lowest occupied molecular orbital (LUMO) excitations) and the active space was chosen to include the highest five occupied orbitals and the lowest five unoccupied orbitals with 10 electrons in 10 orbitals; in other words, a complete active space of (10, 10) was employed. The absorption spectrum was obtained by running molecular dynamics with the OM2 Hamiltonian using a time step of 0.1 fs at 300 K for 10 ps. From each trajectory, 10,000 structures were extracted (one structure every 1 fs of the simulation), and their vertical excitation energies and oscillator strengths were calculated with the OM2/GUGA-CI Hamiltonian. For each excitation energy, the vertical transitions were convoluted with a Lorentzian line shape with a width of 0.001 eV, and all of the resulting Lorentzians were added to yield the excitation spectrum. The width was arbitrarily chosen to get a continuous spectrum; the qualitative shape of the spectrum did not depend on the exact value of the width. Similar OM2/multi-reference configuration interaction (OM2/MRCI) approach were recently used for calculation of the absorption spectrum of methyl hydroperoxide in frozen water clusters [43] and for simulations of dynamics of atmospheric photochemical reactions [58–61].

Table 1. Summary of synthesised (A–I) and purchased (J–L) organic nitrates studied in this work. The first column contains letter abbreviations by which different nitrates are referred to in other tables and figures.

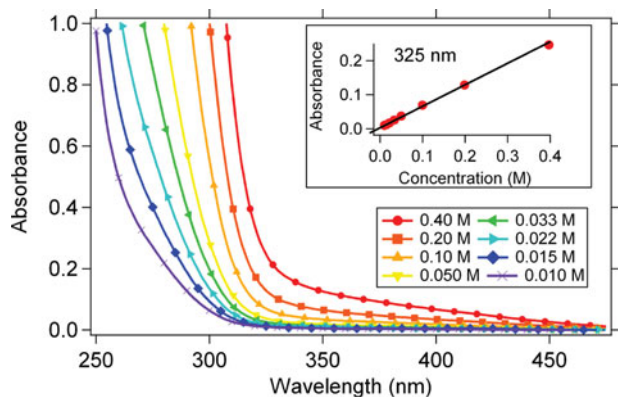|	Structure	Name	Notes
A		2-Hydroxycyclohexyl nitrate	Faint yellow liquid, crystallises
B		3-Hydroxy-3-methylbutan-2-yl nitrate	Acquired colour during storage
C		2-Hydroxyhexyl nitrate	Faint yellow liquid
D		2-Hydroxy-2-methyl-5-(prop-1-en-2-yl)cyclohexyl nitrate	Viscous yellow liquid, crystallises
E		2-Hydroxy-2,6,6-trimethylbicyclo[3.1.1]heptan-3-yl nitrate	Was not able to purify
F		4-Hydroxytetrahydrofuran-3-yl nitrate	Viscous yellowish liquid
G		1-Hydroxybut-3-en-2-yl nitrate	Viscous yellowish liquid
H		2-Hydroxy-1-phenylethyl nitrate	Viscous yellowish liquid
I		2-Hydroxy-3-(nitrooxy)propyl methacrylate	Clear, colourless 'gel'; was not able to purify
J		2-Ethylhexyl nitrate	Commercial
K		Isopropyl nitrate	Commercial
L		Isosorbide mononitrate	Commercial

Figure 1. Representative UV-vis spectra of 2-hydroxycyclohexyl nitrate (compound A) at different solution concentrations. The inset shows an example of calculating the molar absorption coefficient from Beer's law at 325 nm; such calculations have been done at every wavelength for each nitrate investigated in this work.

3. Results and discussion

3.1. Absorption spectra

Figure 1 shows an example of determination of molar absorption coefficients (the terminology follows the recommendations described in Ref. [62]) for 2-hydroxycyclohexyl nitrate (A).

Absorption spectra were recorded at multiple dilution levels in methanol to verify linearity over the experimental range of concentrations. For each wavelength, the molar absorption coefficient was determined by a linear fit of the base-10 absorbance vs. molar concentration, as shown in the inset in Figure 1. The absorbance increases sharply towards the UV range. To avoid deviations from Beer's law, only points with the absorbance values below ∼1 were included in the fit. Table 2 reports the molar absorption coefficients for the examined nitrates between 270 and 330 nm.
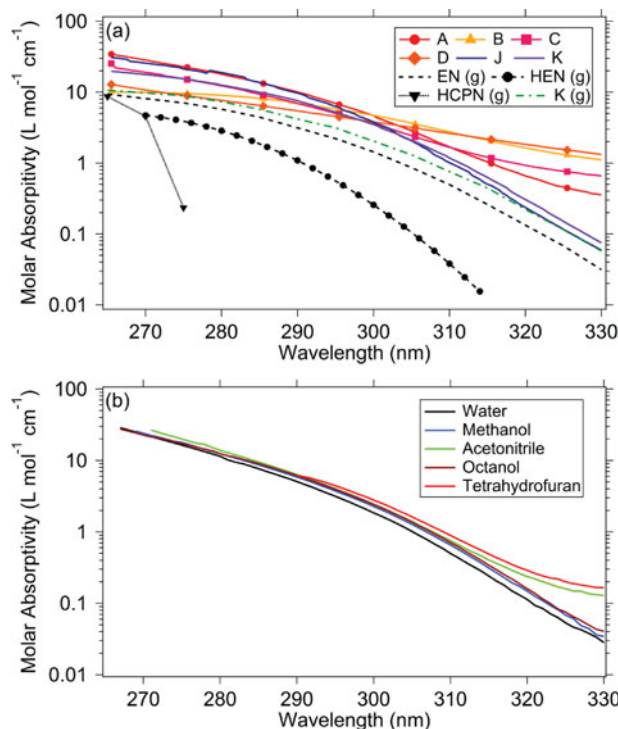

Figure 2. Panel (a): wavelength dependent molar absorption coefficients (molar absorptivity) for β-hydroxyalkyl nitrates A, B, C, D (in various shades of red with markers) and alkyl nitrates J, K (in shades of blue without markers) measured in methanol. Gas-phase data (in black and green) for isopropyl nitrate (K) [63], ethyl nitrate (EN) [63], hydroxyethyl nitrate (HEN) [20], and trans-2-hydroxycyclopentyl-1-nitrate (HCPN) [34] are provided for comparison (only a limited number of points were reported for HCPN). Panel (b) contains the measured molar absorption coefficients for compound L measured in various solvents.

Table 2. Molar absorption coefficients (in L mol^{-1} cm^{-1}) for the investigated nitrates (the labels are defined in Table 1). No data for compounds E and I are included because we could not purify them. The solvent is methanol, except for compound L, which was additionally investigated in water (w), acetonitrile (acn), octanol (oct), and tetrahydrofuran (thf). Each molar absorption coefficient is obtained from a fit of the available absorbance vs. concentration data as shown in Figure 1.

Wavelength (nm)	A	B	C	D	F	H	J	K	L	L$_w$	L$_{acn}$	L$_{oct}$	L$_{thf}$
270	28.43	9.91	19.10	10.76	26.85		25.73	17.80	23.99	23.30		22.71	
275	22.86	9.62	15.50	9.03	22.40		21.34	15.44	17.89	16.49	20.02	17.35	
280	18.00	9.02	12.30	7.64	18.56		18.89	12.55	12.49	11.48	13.85	12.45	
285	13.67	8.18	9.36	6.48	12.97		13.72	9.94	8.68	7.66	9.54	9.02	
290	10.06	6.92	6.94	5.45	10.44	29.74	9.69	7.57	5.87	5.07	6.36	6.16	6.12
295	6.96	5.80	5.03	4.56	8.35	20.22	6.32	5.22	3.75	3.15	4.03	3.96	4.44
300	4.67	4.70	3.56	3.81	6.82	15.45	3.76	3.50	2.27	1.85	2.44	2.42	2.79
305	2.85	3.67	2.44	3.17	5.67	12.41	2.06	2.10	1.28	1.01	1.40	1.37	1.62
310	1.69	2.76	1.67	2.63	4.78	9.99	1.01	1.18	0.66	0.50	0.76	0.71	0.89
315	1.04	2.10	1.21	2.19	4.14	8.30	0.50	0.63	0.31	0.24	0.40	0.34	0.49
320	0.66	1.64	0.93	1.84	3.67	7.10	0.24	0.31	0.15	0.11	0.24	0.16	0.29
325	0.46	1.32	0.77	1.56	3.34	6.16	0.12	0.15	0.07	0.05	0.16	0.08	0.20
330	0.36	1.11	0.66	1.33	3.06	5.29	0.06	0.07	0.03	0.03	0.13	0.04	0.16

We do not report values outside this range because the measured absorbance values were too small for a reliable fit above 330 nm, and there were too few measurement points with acceptably low absorbance below 270 nm. Figure 2(a) compares the molar absorption coefficient for synthesised β-hydroxyalkyl nitrates A, B, C, and D and commercially obtained compounds J and K without the β-hydroxyl group. The values are comparable in the vicinity of 300 nm but diverge at 330 nm, where the absorption coefficients become small and difficult to measure reliably.

Ideally, the measured molar absorption coefficients in solution should be compared to their corresponding gas-phase values. However, gas-phase absorption cross sections for any of the synthesised compounds listed in Table 1 are not available. We are aware of only two gas-phase absorption cross section measurements for β-hydroxyalkyl nitrates, specifically for β-hydroxyethyl nitrate [20] and for trans-2-hydroxycyclopentyl-1-nitrate [34]. The data for both of these β-hydroxyalkyl nitrates are included in Figure 2(a) for comparison. In addition, we include the recommended data [63] for ethyl nitrate and for isopropyl nitrate (K). In all cases, we converted the base e gas-phase absorption cross sections (σ, in cm^2 $molec^{-1}$) to base-10 molar absorption coefficients (ε, in L mol^{-1} cm^{-1}),

$$\varepsilon(\lambda) = \sigma(\lambda) \times \frac{N_A}{1000 \times \ln(10)} \quad (10)$$

where N_A is Avogadro's number.

The direct comparison can only be done for isopropyl nitrate (K), for which the gas-phase molar absorption coefficients are smaller than the ones in methanol by a factor of $\sim$1.6 (Figure 2(a)). The comparison is less straightforward

for other compounds because the absorption coefficients of alkyl nitrates tend to increase with the size of the substituent chain [20–22] and have an unknown dependence on the solvent. However, based on Figure 2(a), the solution-phase absorption coefficients in methanol appear to be larger on average than the gas-phase values. According to the existing gas-phase measurements for β-hydroxyethyl nitrate and ethyl nitrate, the β-hydroxyl group could be expected to have a suppressing effect on the absorption coefficients. However, our measurements indicate that the β-hydroxyl group has a relatively minor effect on the absorption spectrum in solution. The authors of Ref. [20] noted the difficulties of measuring absorption cross sections for β-hydroxy nitrates arising from their low vapour pressure. Indeed, the examination of Figure 2 suggests that the existing absorption cross sections for β-hydroxy nitrates may be underestimated; for example, the low value of the reported 275 nm absorption cross section for trans-2-hydroxycyclopentyl-1-nitrate [34] seems to fall out of the general trend. Therefore, additional measurements of gas-phase absorption cross sections for β-hydroxy nitrates are desirable.

To further investigate the solution effects, we examined absorption spectra of isosorbide mononitrate (L) in various solvents. This compound has two ether groups in β positions, which should have similar electron withdrawing effects on the photochemistry of the nitroxy group as the β-hydroxyl group. Figure 2(b) shows that the absorption spectrum of L does not strongly depend on the type of the solvent across the range of solvent polarities (water, methanol, acetonitrile, octanol, and tetrahydrofuran). The absorption coefficient appears to be systematically smaller in water compared to the less polar solvents in this group

Table 3. Optimised geometries, relative energies, and dipole moments of ethyl nitrate conformers as calculated with MP2/cc-pVDZ.
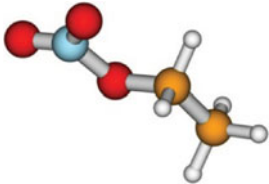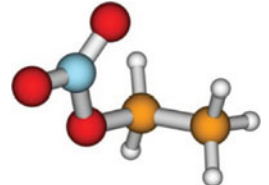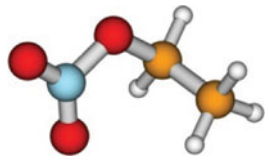
Conformer	Structure	N-O-C-C dihedral angle	Energy (eV)	Dipole moment (debye)	Nomenclature
1		$-180.0°$	0	2.86	anti
2		78.5°	0.005	2.75	gauche +
3		$-78.5°$	0.005	2.75	gauche −

Table 4. The lowest electronic excited states of conformer 1 of ethyl nitrate. All parameters are calculated at CC2 level, but the OM2 energies are also provided for comparison. A similar table for conformer 3 is given in the supporting information section (Table S1).

Electronic state	CC2 energy (eV)	OM2 energy (eV)	Transitions involved	Oscillator strength	Dipole moment (debye)
Ground	0	0	–	–	2.86
1	5.07	4.60	HOMO-2 $\rightarrow$ LUMO 64%	4×10^{-8}	2.34
			HOMO-3 $\rightarrow$ LUMO 31%		
2	6.10	4.87	HOMO-3 $\rightarrow$ LUMO 62%	0.0003	3.44
			HOMO-2 $\rightarrow$ LUMO 23%		
			HOMO-6 $\rightarrow$ LUMO 11%		
3	6.58	5.36	HOMO-1 $\rightarrow$ LUMO 46%	0.080	7.19
			HOMO-5 $\rightarrow$ LUMO 26%		
			HOMO $\rightarrow$ LUMO 16%		
4	7.69	5.39	HOMO $\rightarrow$ LUMO 48%	0.087	1.62
			HOMO-1 $\rightarrow$ LUMO 12%		
			HOMO-2 $\rightarrow$ LUMO + 5 11%		
5	8.19	5.99	HOMO-2 $\rightarrow$ LUMO + 5 22%	0.14	0.88
			HOMO $\rightarrow$ LUMO 16%		
			HOMO-3 $\rightarrow$ LUMO + 5 11%		
			HOMO-2 $\rightarrow$ LUMO + 1 10%		

suggesting a reduction in the excited state dipole moment (confirmed by calculations, see below). However, on the whole, the solvent effect on the absorption spectrum appears to be minimal.

3.2. Computed structures and absorption spectra

The geometries, dihedral angles, relative ground-state energies calculated at the MP2/cc-pVDZ level, and dipole moments of the lowest energy conformers of ethyl nitrate are summarised in Table 3.

The $-ONO_2$ group of all the three conformers is planar; the primary difference between them lies in the N-O-C-C dihedral angle. The conformer 2 (gauche $+$) and conformer 3 (gauche$-$) are stereoisomers, therefore their energies are the same. The conformer 1 is a global minimum at this level of theory, but its energy is within a fraction of a few meV from that of conformers 2 and 3. The vertical excitation energies for conformer 1 calculated at the coupled cluster CC2 level are provided in Table 4, and those for conformer 3 are given in the supporting information Table S1.

The molecular orbitals involved in these transitions are shown in Figure 3 and Figure S2, respectively. The orbitals have similar features but there are subtle differences as well. For example, the first excited state for conformer 3 corresponds mainly to an excitation from HOMO-3 to LUMO, whereas for conformer 1, the main excitation involves HOMO-2 and the LUMO orbital. The lowest electronic exited state of conformer 3 is predicted around 5.07 eV at the CC2 level. For comparison, the first excitation energy is 4.60 eV at the OM2 level. A comparison of the theoretically predicted excitation spectrum to the experimental one shows that the OM2/MRCI method reasonably describes
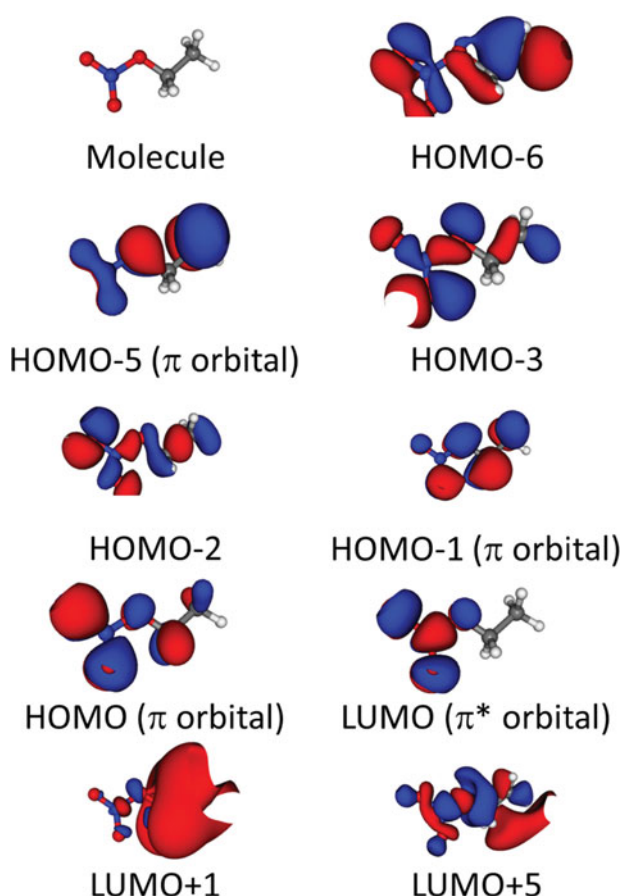

Figure 3. Molecular orbitals (obtained by MP2) involved in electronic transitions of conformer 1 of ethyl nitrate listed in Table 4. A similar figure for conformer 3 is provided in the supporting information section (Figure S2).
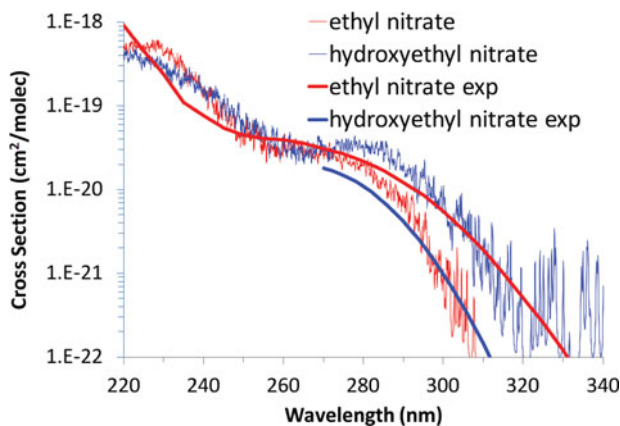
Figure 4. Comparison of theoretically predicted absorption cross sections of ethyl nitrate (red noisy trace) and β-hydroxyethyl nitrate (blue noisy trace). The absorption cross sections for ethyl nitrate (red solid line) [63] and hydroxyethyl nitrate [20] (blue solid line) are shown for comparison. The two theoretical results have been arbitrarily scaled by the same factor. Note that the experiments and simulations predict spectral shifts in the opposite direction for the two compounds.

the actual excitation energies (Figure 4). Normally, the *ab initio* CC2 method is supposed to be more reliable than the OM2/MRCI method. However, in the present case, we suspect that the CC2 states are not covering the relevant orbitals of the different states involved. As a result, we believe that the CC2 calculation is less accurate. An alternative explanation is that this is a case where the multireference description is essential; the semiempirical MRCI has the advantage of more fully covering the active space.

As many as 13 minima were found for β-hydroxyethyl nitrate. Their geometries are shown in Figure S3, and their relative energies and the Boltzmann populations at 300 K are listed in Table 5. The vertical excitation energies at the CC2 level for the lowest energy conformer are provided in Table 6, and Figure S4 shows the corresponding molecular orbitals.

Table 5. Relative energies (as calculated with MP2) and relative Boltzmann populations of β-hydroxyethyl nitrate conformers at 300 K.

Conformer	Energy (eV)	Boltzmann distribution at 300 K (%)
1	0.000	59.5
2	0.020	27.9
3	0.065	4.73
4	0.095	1.53
5	0.108	0.92
6	0.109	0.86
7	0.111	0.80
8	0.113	0.76
9	0.115	0.69
10	0.117	0.64
11	0.117	0.64
12	0.120	0.56
13	0.126	0.46

The lowest electronic exited state is predicted at around 5.09 eV at the CC2 level, which is very similar to the corresponding value for ethyl nitrate. The first excitation energy at the OM2 level (4.59 eV) is also essentially identical to that of ethyl nitrate. However, there are differences between the two systems at higher excitations energies; for example, transition 5 in Table 6 is unique to β-hydroxyethyl nitrate, and is not present in ethyl nitrate. The correspondence between the molecular orbitals of ethyl and β-hydroxyethyl nitrates is shown in Table S2.

The absorption spectra of ethyl nitrate and β-hydroxyethyl nitrate from the MD simulations using the OM2 semiempirical Hamiltonian are shown in Figure 4.

The most important wavelength range for photochemistry in the lower atmosphere is the low energy tail of the absorption spectrum. The oscillator strength for the lowest $n \to \pi^*$ electronic transition responsible for this tail in nitrates is quite low, which is responsible for the increased noise in the predicted spectrum. The calculations predict

Table 6. The electronic excited states of the lowest energy conformer of β-hydroxyethyl nitrate as calculated by CC2. All parameters are calculated at CC2 level, but the OM2 energies are also provided for comparison.

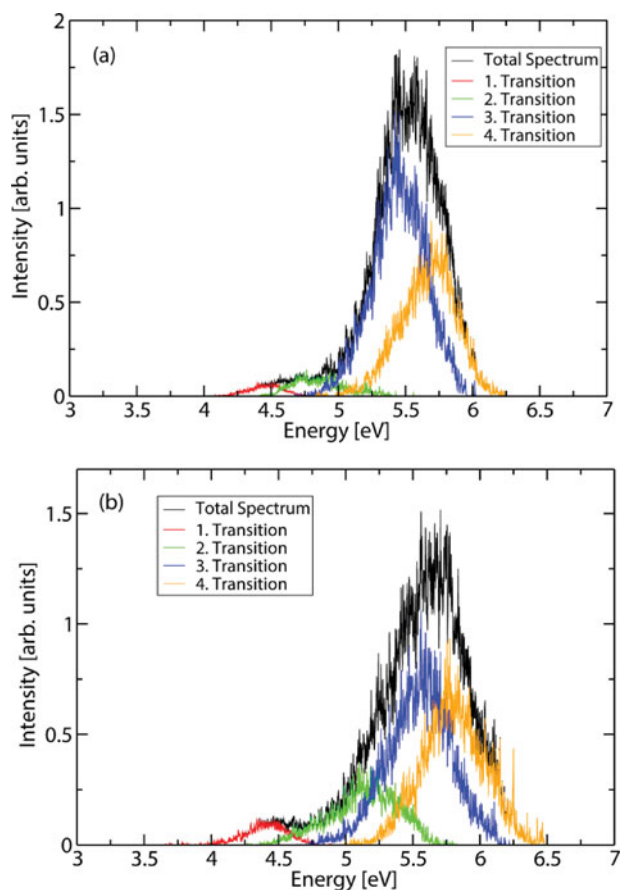| Electronic state	CC2 energy (eV)	OM2 energy (eV)	Main transitions involved	Oscillator strength	Dipole moment (debye)
Ground	0	0	–	–	1.69
1	5.09	4.59	HOMO-4 → LUMO 50% HOMO-3 → LUMO 23% HOMO-2 → LUMO 13%	0.000050	1.35
2	6.12	5.30	HOMO-4 → LUMO 37% HOMO-5 → LUMO 35% HOMO-2 → LUMO 19%	0.000311	2.29
3	6.61	5.59	HOMO-3 → LUMO 47% HOMO-1 → LUMO 11% HOMO-5 → LUMO 11%	0.0721	5.85
4	7.59	5.84	HOMO-1 → LUMO 30%	0.0263	1.81
5	7.96	6.48	HOMO → LUMO 74%	0.0117	13.00

Figure 5. Decomposition of the predicted absorption spectra of ethyl nitrate (a) and β-hydroxyethyl nitrate (b) into contribution from the four lowest electronic states.

a small red shift of the spectrum upon addition of the β-hydroxyl group, whereas the available experiments suggest that the spectrum of β-hydroxyethyl nitrate is slightly blue shifted from the spectrum of ethyl nitrate. However, there is reasonable agreement in the overall shape of the spectra across the entire range over which measurements are available.

We should note that the absorption spectra represent a convolution of different overlapping transitions. Figure 5 shows a decomposition of the predicted absorption spectra of ethyl nitrate and β-hydroxyethyl into contribution from the four lowest electronic states.

The low energy tail of the spectrum is dominated by the lowest electronic state (see Figure 5 and Figure S5). These results demonstrate that the shape of the low energy tail in the spectrum can be adequately predicted by using only one state, which greatly decreases the computational expenses.

4. Photochemical fates of β-hydroxyalkyl nitrates

As discussed in Section 1, the OH reaction is the most important removal mechanism for unsaturated nitrates [33],

but photolysis may become competitive for certain types of saturated nitrate compounds. To examine potential fates of the compounds listed in Table 1, we performed a scaling analysis to determine their most significant atmospheric sinks. This method was previously developed in Refs. [42,64]; therefore, we will only provide a summary of the assumptions used for this particular analysis. Oxidation by OH radicals is typically the most dominant chemical sink for most atmospheric organics in both the aqueous and gaseous phases [65], suggesting that OH oxidation is a reasonable benchmark to determine the significance of direct aqueous photolysis. We chose to compare the rates of chemical reaction via gas-phase photolysis, aqueous-phase photolysis, gas-phase oxidation by OH, and aqueous-phase oxidation by OH. Note that we are not considering loss by dry deposition, which may be an important loss mechanism in the boundary layer. We are also ignoring hydrolysis of hydroxyalkyl nitrate isomers with the nitrate group in the tertiary position, which has been shown to occur with atmospherically relevant rates in both aqueous solutions [66,67] and water-containing aerosols [68].

Henry's Law constant is used to determine the equilibrium partitioning between each phase in an air mass with a specific liquid water content. The parameter 'Z' is defined as the ratio between the gas-phase photolysis rate and the aqueous-phase photolysis rate:

$$Z = \frac{\frac{dn_{h\nu}^{\text{gas}}}{dt}}{\frac{dn_{h\nu}^{\text{aq}}}{dt}} = \frac{J_{\text{gas}}}{J_{\text{aq}}}(R \cdot T \cdot \text{LWC}_v \cdot K_H)^{-1} \qquad (11)$$

where n represents the moles of the compound of interest, t represents time, J is the computed photolysis rate constant using the measured absorption coefficients (see below), R is the gas constant, T is the temperature, LWC_v is the (dimensionless) liquid water content in volume of liquid water per volume of air, and K_H is the Henry's Law constant. The Henry's law constant for isopropyl nitrate was obtained from the experimental measurements of Hauff *et al.* [69]. Henry's law constants of the remaining nitrates were unavailable and thus were predicted from HENRYWIN [70] using bond contribution methods (Table S3). The experimentally measured [35,36] Henry's constants for C2-C5 β-hydroxyalkyl nitrates without other functional groups range from 6×10^3 to 4×10^4 M/atm, which compares reasonably well to the range of HENRYWIN predictions of 3×10^4 to 8×10^4 M/atm for compounds A, B, C, D, E, and G which have no polar functional groups other than hydroxyl and nitroxy. We should note that HENRYWIN Henry's constant predictions of a series of β-hydroxyalkyl nitrates from Ref. [35] overestimated the measured values by factors ranging from 2.6 to 17, so the treatment presented here should be viewed as approximate at best. The method predicts higher solubility for the compound H with an aromatic substituent, which may be an artefact of the bond contribution method.

The highest solubility (1.7×10^{10} M/atm) is predicted for compound L, which has the largest O/C ratio. To investigate the significance of aqueous photochemistry during ideal conditions, we used a cloud liquid water content of 0.5 g m^{-3}, typically the largest value experienced in the troposphere [71].

The aqueous- and gas-phase photolysis rate constants are a function of the actinic flux, the absorption cross section, σ, and the photolysis quantum yield, Φ:

$$\frac{J_{\text{gas}}}{J_{\text{aq}}} = \frac{\int F_A(\lambda) \cdot \Phi_{\text{gas}}(\lambda) \cdot \sigma_{\text{gas}}(\lambda) \cdot d\lambda}{\int F_A(\lambda) \cdot \Phi_{\text{aq}}(\lambda) \cdot \sigma_{\text{aq}}(\lambda) \cdot d\lambda} \quad (12)$$

where λ represents wavelength. Due to the absence of gas-phase absorption cross sections for the investigated compounds, we initially assumed that the gas-phase absorption cross sections were identical to the solution-phase values reported in Table 2. To test the bounds of this framework, we repeated the calculations with a small bathochromic shift in the cross sections. In this variation, gas-phase absorption cross sections were estimated by applying a 10 nm blue shift to the measured cross sections in methanol (Table 2). The application of this 10 nm solvent-induced shift did not significantly affect the conclusions of this analysis. The actinic flux was calculated with the Tropospheric Ultraviolet and Visible (TUV) radiation model [72] at a 24-hr average solar zenith angle of 65º representative of Los Angeles, USA at the summer solstice using a similar procedure described in Ref. [73]. Both aqueous- and gas-phase quantum yields are unknown, but after making the simplification that they are independent of photon energy over the relevant wavelengths (segment of wavelengths where the actinic flux and the absorption cross section are non-zero), we can treat the quantum yields as a ratio. If gas- and aqueous-phase photolysis occur with the same chemical mechanism, we expect that the aqueous-phase quantum yields should be less than or equal to the gas-phase values [42,64]. In certain cases, gas- and aqueous-phase photolysis mechanisms may differ significantly, leading to a breakdown in this assumption [74]. If the gas-phase and aqueous-phase quantum yields are of the same magnitude, the simplified factor Z reveals the significance of aqueous-phase photolysis relative to gas-phase photolysis.

We can also compare the rate of aqueous photolysis with the rate of aqueous oxidation by OH by defining a factor Q:

$$Q = \frac{\frac{dn_{\text{OH}}^{\text{aq}}}{dt}}{\frac{dn_{\text{h}\nu}^{\text{aq}}}{dt}} = \frac{k_{\text{OH}}[\text{OH}]}{J_{\text{aq}}} \quad (13)$$

where k_{OH} is the rate constant for aqueous oxidation by OH. The values of k_{OH} are not available experimentally in the literature, so we used group contribution structure–activity relationships (SAR) that were developed to predict values for alkyl nitrates [75]. We tested these SARs us-
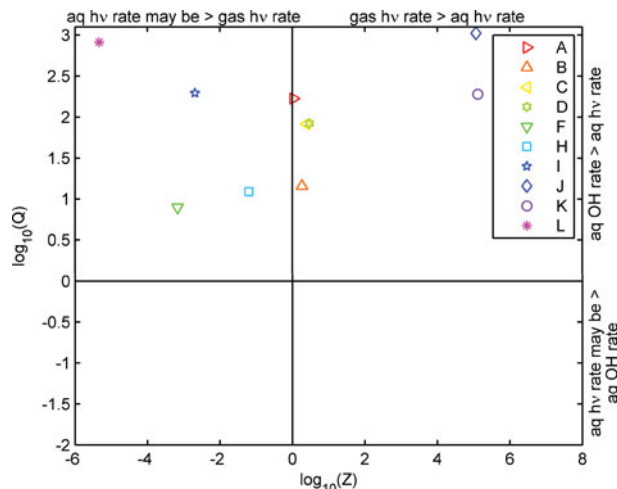

Figure 6. Likely photo-induced atmospheric sinks of studied compounds at a solar zenith angle of 65°. Q is defined as the ratio of the aqueous oxidation by OH rate and the aqueous photolysis rate. Z is defined as the ratio of the gas photolysis rate and aqueous photolysis rate. The lack of points with $Q < 1$ and $Z < 1$ indicates that liquid-phase photolysis of nitrate compounds considered in this work is too slow relative other sink processes under typical atmospheric conditions.

ing experimental data from Ref. [17] for two hydroxyl nitrates: E-2-methyl-4-nitrooxybut-2-ene-1-ol and 3-methyl-2-nitroxybut-3-ene-1-ol. While SARs did a reasonable job predicting the rate constants for the aqueous reaction of OH with simpler alkyl nitrates, SARs overpredicted the rate constants for these two compounds by a factor of 23 and 57, respectively. Therefore, this SAR is satisfactory for the purposes of examining the relative influence of aqueous photolysis but may be an order of magnitude off with respect to the absolute rate of reactions with OH. Aqueous OH concentrations were set to 10^{-13} M, the daytime cloud-water value estimated in Ref. [76]. To understand the maximum contribution of aqueous photolysis, the unknown aqueous photolysis quantum yields were set to unity. Comparison of Z and Q on the same axis can illustrate the potential significance of aqueous photolysis. Figure 6 reveals that for the nine compounds with measured absorption coefficients, aqueous oxidation by OH is significantly faster than aqueous photolysis even under conditions that will lead to an enhancement in aqueous photolysis rates (wet clouds, strong actinic radiation, and large aqueous photolysis quantum yields).

Depending on the compound and the ratio in quantum yields, aqueous photolysis may be faster than gaseous photolysis, but in all cases, oxidation by OH appears to be the dominant photo-induced sink. Comparison of predicted and measured Henry's law constants and k_{OH} values of a few similar compounds indicates that there is the potential that each of these values may be overestimated by the predictive methods we employed. A potential overestimation in the Henry's law constant does not affect the overall

conclusions, as the studied compounds could be less soluble than predicted. However, an overestimation in k_{OH} values would suppress the significance of aqueous photolysis and could potentially modify the conclusion that aqueous photolysis is not a significant sink.

5. Conclusions

The following conclusions emerge based on the measurements, calculations, and simulations carried out in this paper:

The main question posed by this paper was whether the direct photolysis of β-hydroxyalkyl nitrates in the aqueous phase or in the organic particle phase is atmospherically relevant. Results of this work suggest that the answer to this question is 'no'. Unlike the β-carbonyl group [33], the β-hydroxyl group appears to have a relatively minor effect on the absorption coefficients of organic nitrates in methanol, and by extension, in an aqueous solution. Therefore, it is unlikely that the photochemical loss of β-hydroxyalkyl nitrates will accelerate once they partition in cloud droplets or aerosol particles. A more quantitative analysis of the relative rates of loss of nitrates by gas-phase and aqueous-phase oxidation confirms that direct aqueous photolysis is not likely to compete with gas-phase oxidation and photolysis, and with aqueous-phase oxidation by OH.

The absorption coefficients of organic nitrates appear to increase slightly in solutions relative to the gas phase. However, the effect is not dramatic. Therefore, it should be reasonable to approximate gas-phase absorption coefficients by solution-based measurements, and vice versa. This should simplify measurements for nitrates that have low volatility (and hence cannot be studied by gas-phase techniques) or low solubility (cannot be studied by solution-based methods).

The OM2/GUGA-CI computational approach utilised in this work provides reasonable predictions for the wavelength dependence of the absorption spectra of organic nitrates. The qualitative agreement for the shape of the red tail of the absorption spectrum, which plays an important role in photochemistry of nitrates in the lower atmosphere, is especially noteworthy. The utility of this method needs to be investigated further for predicting the shapes of absorption tails of other atmospherically relevant organic molecules, such as peroxides, carbonyls, and multifunctional compounds.

Disclosure statement

No potential conflict of interest was reported by the authors.

Funding

Supplemental data

Supplemental data for this article can be accessed at http://dx.doi.org/10.1080/00268976.2015.1017020.

ORCID

Sergey A. Nizkorodov http://orcid.org/0000-0003-0891-0052

References

[1] B.J. Finlayson-Pitts and J.N. Pitts, *Chemistry of the Upper and Lower Atmosphere: Theory, Experiments, and Applications* (Academic Press, San Diego, CA, 2000).

[2] J.M. O'Brien, E. Czuba, D.R. Hastie, J.S. Francisco, and P.B. Shepson, J. Phys. Chem. A **102**, 8903 (1998).

[3] S.X. Ma, J.D. Rindelaub, K.M. McAvey, P.D. Gagare, B.A. Nault, P.V. Ramachandran, and P.B. Shepson, Atmos. Chem. Phys. **11**, 6337 (2011).

[4] G. Werner, J. Kastler, R. Looser, and K. Ballschmiter, Angew. Chem. Int. Ed. **38**, 1634 (1999).

[5] A. Matsunaga and P.J. Ziemann, Proc. Nat. Acad. Sci. U.S.A. **107**, 6664 (2010).

[6] J.M. O'Brien, P.B. Shepson, Q. Wu, T. Biesenthal, J.W. Bottenheim, H.A. Wiebe, K.G. Anlauf, and P. Brickell, Atmos. Environ. **31**, 2059 (1997).

[7] M.R. Beaver, J.M.S. Clair, F. Paulot, K.M. Spencer, J.D. Crounse, B.W. LaFranchi, K.E. Min, S.E. Pusede, P.J. Wooldridge, G.W. Schade, C. Park, R.C. Cohen, and P.O. Wennberg, Atmos. Chem. Phys. **12**, 5773 (2012).

[8] R.G. Fischer, J. Kastler, and K. Ballschmiter, J. Geophys. Res. D **105**, 14473 (2000).

[9] A.E. Perring, T.H. Bertram, P.J. Wooldridge, A. Fried, B.G. Heikes, J. Dibb, J.D. Crounse, P.O. Wennberg, N.J. Blake, D.R. Blake, W.H. Brune, H.B. Singh, and R.C. Cohen, Atmos. Chem. Phys. **9**, 1451 (2009).

[10] K.A. Pratt, L.H. Mielke, P.B. Shepson, A.M. Bryan, A.L. Steiner, J. Ortega, R. Daly, D. Helmig, C.S. Vogel, S. Griffith, S. Dusanter, P.S. Stevens, and M. Alaghmand, Atmos. Chem. Phys. **12**, 10125 (2012).

[11] A.W. Rollins, A. Kiendler-Scharr, J.L. Fry, T. Brauers, S.S. Brown, H.P. Dorn, W.P. Dube, H. Fuchs, A. Mensah, T.F. Mentel, F. Rohrer, R. Tillmann, R. Wegener, P.J. Wooldridge, and R.C. Cohen, Atmos. Chem. Phys. **9**, 6685 (2009).

[12] A.E. Perring, A. Wisthaler, M. Graus, P.J. Wooldridge, A.L. Lockwood, L.H. Mielke, P.B. Shepson, A. Hansel, and R.C. Cohen, Atmos. Chem. Phys. **9**, 4945 (2009).

[13] M. Spittler, I. Barnes, I. Bejan, K.J. Brockmann, T. Benter, and K. Wirtz, Atmos. Environ. **40**, S116 (2006).

[14] J.L. Fry, A. Kiendler-Scharr, A.W. Rollins, P.J. Wooldridge, S.S. Brown, H. Fuchs, W. Dube, A. Mensah, M. dal Maso, R. Tillmann, H.P. Dorn, T. Brauers, and R.C. Cohen, Atmos. Chem. Phys. **9**, 1431 (2009).

[15] I. Waengberg, I. Barnes, and K.H. Becker, Environ. Sci. Technol. **31**, 2130 (1997).

[16] M. Hallquist, I. Waengberg, E. Ljungstroem, I. Barnes, and K.-H. Becker, Environ. Sci. Technol. **33**, 553 (1999).

[17] L. Lee, A.P. Teng, P.O. Wennberg, J.D. Crounse, and R.C. Cohen, J. Phys. Chem. A **118**, 1622 (2014).

[18] L. Zhu and D. Kellis, Chem. Phys. Lett. **278**, 41 (1997).

[19] R.K. Talukdar, J.B. Burkholder, M. Hunter, M.K. Gilles, J.M. Roberts, and A.R. Ravishankara, J Chem. Soc. Faraday Trans. **93**, 2797 (1997).

[20] J.M. Roberts and R.W. Fajer, Environ. Sci. Technol. **23**, 945 (1989).

[21] M.P. Turberg, D.M. Giolando, C. Tilt, T. Soper, S. Mason, M. Davies, P. Klingensmith, and G.A. Takacs, J. Photochem. Photobiol. A **51**, 281 (1990).

[22] K.C. Clemitshaw, J. Williams, O.V. Rattigan, D.E. Shallcross, K.S. Law, and R.A. Cox, J Photochem. Photobiol. A Chem. **102**, 117 (1997).

[23] I. Barnes, K.H. Becker, and T. Zhu, J. Atm. Chem. **17**, 353 (1993).

[24] W. Luke, R.R. Dickerson, and L.J. Nunnermacker, J. Geophys. Res. D **94**, 14905 (1989).

[25] P.G. Carbajo and A.J. Orr-Ewing, Phys. Chem. Chem. Phys. **12**, 6084 (2010).

[26] L.E. Harris, J. Chem. Phys. **58**, 5615 (1973).

[27] L.E. Harris, Nature **243**, 103 (1973).

[28] T.F. Shamsutdinov, D.V. Chachkov, A.G. Shamov, and G.M. Khrapkovskii, Izvestiya Vysshikh Uchebnykh Zavedenii, Khimiya i Khimicheskaya Tekhnologiya **49**, 38 (2006).

[29] G.M. Khrapkovskii, T.F. Shamsutdinov, D.V. Chachkov, and A.G. Shamov, J. Mol. Struct. THEOCHEM **686**, 185 (2004).

[30] I.V. Schweigert and B.I. Dunlap, J. Chem. Phys. **130**, 244110/1 (2009).

[31] E.L. Derro, C. Murray, M.I. Lester, and M.D. Marshall, Phys. Chem. Chem. Phys. **9**, 262 (2007).

[32] J. Soto, D. Pelaez, J.C. Otero, F.J. Avila, and J.F. Arenas, Phys. Chem. Chem. Phys. **11**, 2631 (2009).

[33] J.F. Müller, J. Peeters, and T. Stavrakou, Atmos. Chem. Phys. **14**, 2497 (2014).

[34] I. Waengberg, I. Barnes, and K.H. Becker, Chem. Phys. Lett. **261**, 138 (1996).

[35] P.B. Shepson, E. Mackay, and K. Muthuramu, Environ. Sci. Technol. **30**, 3618 (1996).

[36] K. Treves, L. Shragina, and Y. Rudich, Environ. Sci. Technol. **34**, 1197 (2000).

[37] T.B. Nguyen, P.J.L. Roach, J.A. Laskin, and S.A. Nizkorodov, Atmos. Chem. Phys. **11**, 6931 (2011).

[38] T.B. Nguyen, J. Laskin, A. Laskin, and S.A. Nizkorodov, Environ. Sci. Technol. **45**, 6908 (2011).

[39] Y. Yu, M.J. Ezell, A. Zelenyuk, D. Imre, L. Alexander, J. Ortega, B. D'Anna, C.W. Harmon, S.N. Johnson, and B.J. Finlayson-Pitts, Atmos. Environ. **42**, 5044 (2008).

[40] J. Matthews, A. Sinha, and S. Francisco Joseph, PNAS **102**, 7449 (2005).

[41] M. Ončák, P. Slavíček, M. Fárník, and U. Buck, J. Phys. Chem. A **115**, 6155 (2011).

[42] S.A. Epstein, E. Tapavicza, F. Furche, and S.A. Nizkorodov, Atm. Chem. Phys. Discuss. **13**, 10905 (2013).

[43] S.A. Epstein, D. Shemesh, V.T. Tran, S.A. Nizkorodov, and R.B. Gerber, J. Phys. Chem. A **116**, 6068 (2012).

[44] R.B. Gerber, D. Shemesh, M.E. Varner, J. Kalinowski, and B. Hirshberg, Phys. Chem. Chem. Phys. **16**, 9760 (2014).

[45] V.M. Csizmadia, S.A. Houlden, G.J. Koves, J.M. Boggs, and I.G. Csizmadia, J. Org. Chem. **38**, 2281 (1973).

[46] D. O'Sullivan, R.P. McLaughlin, K.C. Clemitshaw, and J.R. Sodeau, J. Phys. Chem. A **118**, 9890 (2014).

[47] B. Das, M. Krishnaiah, K. Venkateswarlu, and V.S. Reddy, Helv. Chim. Acta **90**, 110 (2007).

[48] E.A. Bruns, V. Perraud, A. Zelenyuk, M.J. Ezell, S.N. Johnson, Y. Yu, D. Imre, B.J. Finlayson-Pitts, and M.L. Alexander, Environ. Sci. Technol. **44**, 1056 (2010).

[49] *Avogadro: An Open-Source Molecular Builder and Visualization Tool*. Version 1. <http://avogadro.openmolecules.net/> (accessed February 21, 2015).

[50] M.D. Hanwell, D.E. Curtis, D.C. Lonie, T. Vandermeersch, E. Zurek, and G.R. Hutchison, J. Cheminform. **4**, 17 (2012).

[51] F. Weigend and M. Häser, Theor. Chem. Acc. **97**, 331 (1997).

[52] T.H. Dunning, J. Chem. Phys. **90**, 1007 (1989).

[53] O. Christiansen, H. Koch, and P. Jorgensen, Chem. Phys. Lett. **243**, 409 (1995).

[54] C. Hättig and F. Weigend, J. Chem. Phys. **113**, 5154 (2000).

[55] W. Weber and W. Thiel, Theor. Chem. Acc. **103**, 495 (2000).

[56] A. Koslowski, M.E. Beck, and W. Thiel, J. Comput. Chem. **24**, 714 (2003).

[57] W. Thiel, *MNDO Program, Version 6.1* (Max-Planck-Institut für Kohlenforschung, Mülheim an der Ruhr, Germany, 2007).

[58] D. Shemesh, S.L. Blair, R.B. Gerber, and S.A. Nizkorodov, Phys. Chem. Chem. Phys. **16**, 23861 (2014).

[59] D. Shemesh, Z.G. Lan, and R.B. Gerber, J. Phys. Chem. A **117**, 11711 (2013).

[60] H. Lignell, S.A. Epstein, M.R. Marvin, D. Shemesh, B. Gerber, and S. Nizkorodov, J. Phys. Chem. A **117**, 12930 (2013).

[61] D. Shemesh and R.B. Gerber, Mol. Phys. **110**, 605 (2012).

[62] S.E. Braslavsky, Pure Appl. Chem. **79**, 293 (2007).

[63] R. Atkinson, D.L. Baulch, R.A. Cox, J.N. Crowley, R.F. Hampson, R.G. Hynes, M.E. Jenkin, M.J. Rossi, J. Troe, and I. Subcommittee, Atmos. Chem. Phys. **6**, 3625 (2006).

[64] S.A. Epstein and S.A. Nizkorodov, Atmos. Chem. Phys. **12**, 8205 (2012).

[65] B. Ervens, S. Gligorovski, and H. Herrmann, Phys. Chem. Chem. Phys. **5**, 1811 (2003).

[66] K.S. Hu, A.I. Darer, and M.J. Elrod, Atmos. Chem. Phys. **11**, 8307 (2011).

[67] A.I. Darer, N.C. Cole-Filipiak, A.E. O'Connor, and M.J. Elrod, Environ. Sci. Technol. **45**, 1895 (2011).

[68] S. Liu, J.E. Shilling, C. Song, N. Hiranuma, R.A. Zaveri, and L.M. Russell, Aerosol Sci. Technol. **46**, 1359 (2012).

[69] K. Hauff, R.G. Fischer, and K. Ballschmiter, Chemosphere **37**, 2599 (1998).

[70] US EPA. *Estimation Programs Interface (EPI) Suite*. (United States Environmental Protection Agency, Washington, DC, 2012). <http://www.epa.gov/opptintr/exposure/pubs/episuite.htm>.

[71] P.V. Hobbs, *Aerosol–Cloud–Climate Interactions* (Academic Press, San Diego, CA, 1993).

[72] S. Madronich, S. Flocke, J. Zeng, I. Petropavlovskikh, and J. Lee-Taylor, *Tropospheric Ultraviolet and Visible (TUV) Radiation Model* (National Center for Atmospheric Research, 2014). <http://cprm.acd.ucar.edu/Models/TUV/Interactive_TUV/>.

[73] S.A. Epstein, S.L. Blair, and S.A. Nizkorodov, Environ. Sci. Technol. **48**, 11251 (2014).

[74] A.E. Reed Harris, B. Ervens, R.K. Shoemaker, J.A. Kroll, R.J. Rapf, E.C. Griffith, A. Monod, and V. Vaida, J. Phys. Chem. A **118**, 8505 (2014).

[75] D. Minakata, K. Li, P. Westerhoff, and J. Crittenden, Environ. Sci. Technol. **43**, 6220 (2009).

[76] B. Ervens, B.J. Turpin, and R.J. Weber, Atmos. Chem. Phys. **11**, 11069 (2011).